Crumpling Defective Graphene Sheets

Yangchao Liao a, Zhaofan Li a, Andrew B. Croll b,c, and Wenjie Xia a,c,*

^a Department of Civil, Construction and Environmental Engineering, North Dakota State
University, Fargo, North Dakota 58108, United States

Department of Physics, North Dakota State University, Fargo, North Dakota 58108, United
 States

Materials and Nanotechnology, North Dakota State University, Fargo, North Dakota 58108,
 United States

* To whom correspondence should be addressed.

Contact information: wenjie.xia@ndsu.edu

ABSTRACT

Upon crumpling, graphene sheets yield intriguing hierarchical structures with high resistance to

compression and aggregation, garnering a great deal of attention in recent years for their

remarkable potential in a variety of applications. Here, we aim to understand the effect of Stone-

Wales (SW) defects, i.e., a typical topological defect of graphene, on the crumpling behavior of

graphene sheets at a fundamental level. By employing atomistically informed coarse-grained

molecular dynamics (CG-MD) simulations, we find that SW defects strongly influence the sheet

conformation as manifested by the change in size scaling laws and weaken the self-adhesion of

the sheet during the crumpling process. Remarkably, the analyses of the internal structures (i.e.,

curvatures, stresses, and cross-section patterns) of crumpled graphene emphasize the enhanced

mechanical heterogeneity and "glass-like" amorphous state elicited by SW defects. Our findings

pave the way for understanding and exploring the tailored design of crumpled structure via defect

engineering.

KEYWORDS: Coarse-Grained Modeling, Stone–Wales Defect, Crumpled Graphene, Structural

Behavior, Mechanical State, Molecular Dynamics Simulations

2

Graphene, a one-atom thick two-dimensional (2D) hexagonal lattice composed of carbon atoms covalently bonded via sp²-orbitals, has promoted research in the fields of materials science and condensed matter physics in recent years owing to its remarkable mechanical,2 thermal,3 electronic, and magnetic properties. Interestingly, thermal motion causes free-floating graphene sheets to spontaneously develop distinct corrugations and crumples, rather than maintaining a perfectly flat configuration.⁶ Given the relatively low out-of-plane stiffness of atomically thick graphene sheets, they typically exhibit wrinkling and crumpling in preparation, transfer, and application when subjected to intermolecular and interfacial interactions, as well as when their aspect ratio exceeds a certain critical value, 8 or when their structure is defective. 9,10,11 Despite the highly complex internal structure of corrugated and crumpled graphene, especially for graphene crumpled spheres, they are ultimately comprised of a handful of building block structures, such as bends, ¹² folds, ¹³ developable cones, ¹⁴ and stretching ridges. ¹⁵ The stochastic combination of these micro/nano building blocks with spatially periodic or nonperiodic topology significantly affects the mechanical, and electrical properties of the crumpled system, and therefore, it is critical to gain insights into the structure-property relationships of crumpled graphene sheets.

Recently, considerable efforts have been made to explore the crumpling behavior along with the intriguing properties of graphene-based materials.^{6,16} In general, the crumpling behavior of graphene sheets under hydrostatic pressure can be summarized as a process of edge bending to random folding and then to high compacting.^{17,18,19,20} This crumpling process is found to be largely influenced by the sheet properties (e.g., geometry^{19,20}, defects,^{21,22,23} and stickiness^{24,25}) and the environmental conditions (e.g., temperature^{20,26} and solvent^{27,28,29}), resulting in crumpled systems having diverse packing efficiencies and unique internal structures. Attractively, the crumpled graphene sheets possess improved compressive strength,³⁰ thermal diffusivity,³¹ stability and

dispersibility (resistance to aggregation),³² and electron mobility and energy gap,³³ along with superhydrophobicity and tunable wettability and transmittance,⁷ which are ideal for applications in composites,^{34,35} sensors,³⁶ electronics,³⁷ energy storage^{38,39}, biomedicine⁴⁰, and friction and wear reduction.⁴¹

Of concern is that many physical properties and applications of crumpled graphene depend strongly on its crumpled morphology, such as overall size, degree of crumpling, and internal structures. 6,16 Further, the effect of topological defects on the crumpled morphology of graphene cannot be underestimated among numerous influencing factors. A series of studies suggested that topological defects, such as Stone-Wales (SW) defects, 42,43 divacancies, 44 grain boundaries, 45 and dislocations, 46 cause the local lattice of graphene to distort and deform, which further allow the system to reach the lowest energy state, resulting in graphene sheets exhibiting various degrees of wrinkling and crumpling. 9,10,11,47,48 Usually, graphene sheets bear certain defects due to the limitations of the preparation technology; defects can be artificially introduced into graphene by several methods, for example, proton irradiation, ⁴⁹ electron beam, ⁵⁰ and ion bombardment. ⁵¹ It is increasingly critical to investigate corrugated and crumpled graphene sheets of large size and defect degree, benefiting from the successful synthesis of stand-alone centimeter-scale single-layer truly amorphous graphene in recent years.⁵² To date, many studies have explored the structural behavior of graphene-based sheets with different properties in various crumpling environments. 17,19,20,22,23,24,29,30,53 However, in-depth understanding of the crumpling behavior and internal structure of amorphous graphene due to SW defects are still significantly limited.

In this study, we systematically investigate the crumpling behavior and internal structure of SW defected graphene sheets by employing the coarse-grained (CG) molecular dynamics (MD) simulations.⁵⁴ The CG model is derived from the all-atomistic (AA) graphene model using the

strain-energy conservation approach with a 4-to-1 mapping scheme maintaining a hexagonal lattice geometry (Figure 1a). To obtain the SW defect structure, 42,43,55 the bond of CG model can be intentionally rotated by 90° around the center of the bond, which transforms four hexagons into two pentagons and heptagons (Figure 1b). Note that various amounts of defect sites with different orientations were randomly selected throughout the graphene sheet, leading to defect ratios ranging from 0 to 0.14. Furthermore, the square CG graphene models studied here have edge lengths L ranging from 10.3 nm to 100.6 nm, and the SW defect ratios p considered ranging from 0 to 0.14. Specifically, $p = 2n_{sw}/N$, where N and n_{sw} are the total number of sheet beads and total number of SW defects, respectively. In particular, the compacting of the CG sheet model by a confining sphere of variable radius R_c (Figure 1c) is simulated to mimic the crumpling process of the sheet based on the aerosol evaporation method in the experiment. ^29,32,56 The compaction ratio $\rho_{\rm c}=$ $R_{\rm c}/R_{\rm c0}$ ($\rho_{\rm c} \leq 1$, $\rho_{\rm c} = 1$ and indicates the sheet in initial equilibrium) is introduced here to describe the crumpling degree of the sheet, where R_{c0} is the initial radius of the confining sphere. Further details of the CG model and MD simulations are given in the Supporting Information and in previous studies. 19,24,25,30,54

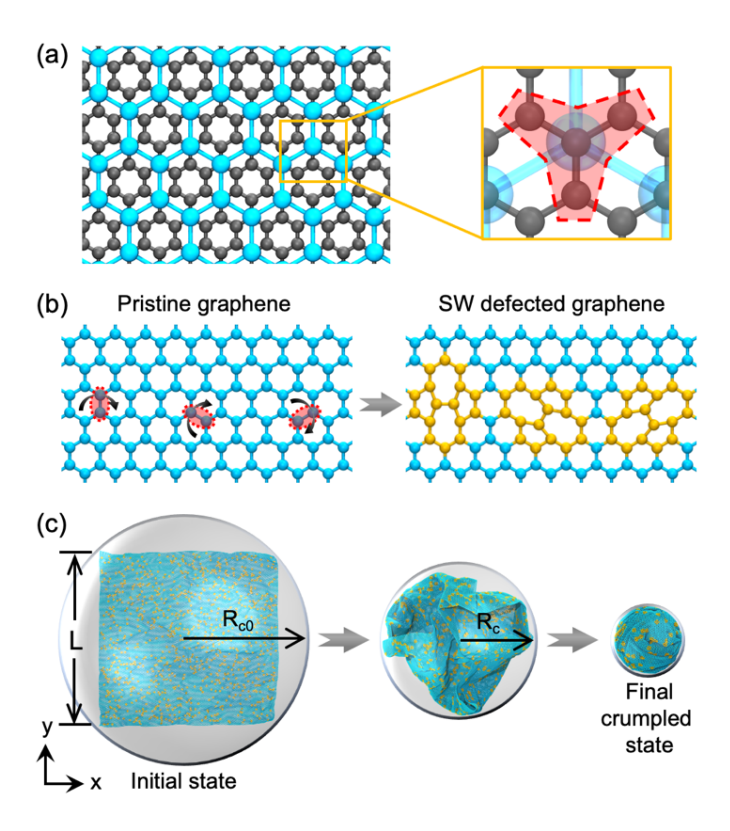


Figure 1. (a) A 4-to-1 mapping scheme for the CG graphene model, where four connected carbon atoms of the AA model (the black atoms highlighted in the pink region in the zoom-in) are represented by a CG bead (cyan bead). (b) Schematic illustration of SW defects with different orientations in CG graphene sheet. For the SW defect, the bond between the two CG beads is rotated by 90° to transform four hexagons into two pentagons and heptagons (yellow beads). (c) Schematic illustration of the MD simulation of the crumpling process. The SW defected graphene sheet with side length L is confined by a confining sphere, and R_{c0} and R_{c} are the radii of the confining sphere in the initial state and during the crumpling process, respectively.

We first discuss the effectiveness of the CG graphene model in simulating SW defects. Then, the effect of SW defect ratios on the fractal dimension and Flory exponent of graphene sheets in equilibrium is determined by analyzing the radius of gyration, hydrodynamic radius, and intrinsic viscosity of the system. Next, by evaluating the total potential energy and shape descriptors of the system during the crumpling process, we find that SW defects significantly affect the sheet crumpling behavior by weakening its self-adhering and self-folding behaviors. Finally, the local

curvature, local stress, cross-section pattern, and order parameter of the cross-section of the sheets in the final crumpled state (crumpled spheres) are analyzed to uncover the mechanical heterogeneity and amorphous structure arising from the SW defects.

Defective graphene conformation. We first investigate the conformational features of CG graphene sheets (L = 100.6 nm) with various SW defect ratios p in the initial equilibrium (i.e., without crumpling). It is observed that the sheets with SW defects exhibit significant corrugations compared to the pristine graphene sheet (p = 0) having a relatively flat conformation, and the corrugation intensifies with increasing p (Figure 2a). Meanwhile, the analyses of the local out-ofplane displacement h_i distribution (Figure 2b) and the local curvature distribution (Figure S1 in the Supporting Information) show that the large out-of-plane buckling region of the sheet increases with increasing p. Such corrugation can be quantified by the corrugation amplification factor (CAF), which is defined as the ratio of the height fluctuations of any system relative to pristine graphene and can be used to assess the impact of defects on the corrugation of graphene. Figure 2c shows that the CAF is overall exponentially related to p; the CAF increases significantly with increasing p when $p \le 0.03$ (i.e., regime 1), while it gradually converges to values of ~3 to 3.7 when $p \gtrsim 0.03$ (i.e., regime 2). These two different regimes could be attributed to defect-induced percolation behavior; the defects could form a connected network which spans the sheet. 57,58,59 In brief, when p is small, the degree of network connectivity of the corrugation is relatively low, making the CAF more sensitive to the influence of p; as p becomes larger, this connectivity is basically saturated and its CAF does not vary significantly. On a hexagonal lattice one might expect a bond percolation threshold of 0.65. On our lattices each SW defect affects of order 10 bonds, so we would expect the threshold to occur near $p\sim0.065$ near where we observe the transition to regime 2.

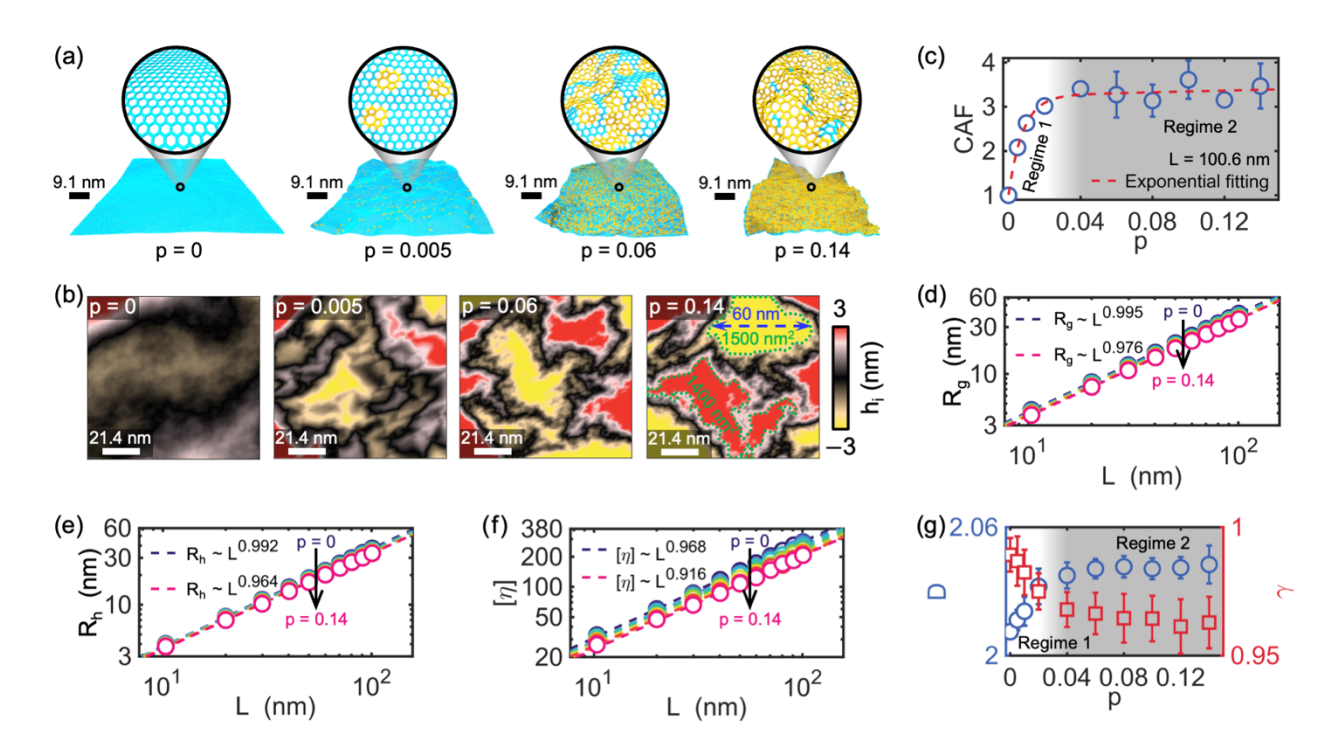


Figure 2. (a) Representative configurations and (b) local out-of-plane displacement h_i distributions of graphene sheets with L=100.6 nm having various SW defect ratios p in the initial equilibrium. The zoom-ins in panel (a) show the detailed distortion of the graphene lattice (with defect-free and SW defects). In panel (b) with p=0.14, the areas of the yellow and red regions enclosed by the green dotted lines are around 1500 nm² and 1400 nm², respectively, and the blue dashed double-arrow marks the dimension of this yellow region as about 60 nm in the horizontal direction. The black line in panel (a) and white line in panel (b) represent the scale bar. (c) Corrugation amplification factor (CAF) as a function of p for graphene sheets with L=100.6 nm. The red dashed line represents the exponential fitting. Power-law scaling relationships between the length L of sheets with different p and the (d) radius of gyration R_g , (e) hydrodynamic radius R_h , and (f) intrinsic viscosity $[\eta]$ of the sheets, respectively, in initial equilibrium. The dashed lines show the fitting, and the solid arrow marks the direction of increase of p. (g) Variation of fractal dimension D and Flory exponent p of graphene sheets with varying p. Five independent simulations are performed to obtain the average values of CAF, R_g , R_h , $[\eta]$, D, and p for graphene sheets with different SW defects features. Details on the calculation of h_i , CAF, R_g , R_h , and $[\eta]$ are given in the Supporting Information and in previous studies.

This phenomenon verifies the direct influence of SW defects on the corrugation conformation of simulated defected CG graphene model, which is primarily due to the local

distortion and deformation of the SW defective lattice to reach the lowest energy state. This observation is similar to the one with reconstructed vacancy (RV) defect,³⁰ resulting in the sheet moving out of plane. Our results are consistent with the distortion and corrugation phenomenon of SW defects reported in previous studies,^{11,42,43,61,62} and the obtained CAF is in good agreement with the results of the machine learning-based MD simulations.¹¹ It is evident that the SW defected graphene model built based on previously developed CG model⁵⁴ can effectively capture the essential conformational features (e.g., corrugations) influenced by defects. More importantly, it can be observed from Figure 2b that the area of the continuous region of the maximum and minimum h_i approaches 1400 nm² and 1500 nm², respectively (approximately the area of a square sheet with L = 38 nm), spanning up to 60 nm. However, this feature cannot be well captured in atomistic modeling because of its spatiotemporal limits. This necessitates the CG model used in this work to study the SW defect by considering such size effects, with greatly improved the computational efficiency.^{19,54}

We further explore the effect of SW defects on the conformational scaling laws of graphene sheets in equilibrium. It can be found that the radius of gyration $R_{\rm g}$ (Figure 2d), hydrodynamic radius $R_{\rm h}$ (Figure 2e), and intrinsic viscosity $[\eta]$ (Figure 2f) of the sheets at various defect ratios p obey the scaling laws $R_{\rm g} \propto L^{2/D}$, 63 $R_{\rm h} \propto L^{v_{\rm h}}$, 63 and $[\eta] \propto L^{3\gamma-2}$, 28 respectively; here, D, $v_{\rm h}$, and γ are the fractal dimension, the scaling exponent of $R_{\rm h}$, and the Flory exponent of $[\eta]$, respectively. It is noticeable that $R_{\rm g}$, $R_{\rm h}$, and $[\eta]$ all tend to decrease as p rises, caused by the significant wrinkling and crumpling in sheets with large defect ratios. Moreover, the scaling exponent $v_{\rm h}$ of $R_{\rm h}$ obtained here is substantially smaller than the scaling exponent 2/D of $R_{\rm g}$, which is consistent with previous findings. 28,63 On the other hand, D and γ of the sheets show increasing and decreasing trends with increasing p, respectively (Figure 2g). Analogous to CAF (Figure 2c), the

trends in D and γ can be divided into two regimes, i.e., drastic changes within regime 1 and a leveling off within regime 2, which can also be attributed to the defect-induced percolation. It is to be noted that the D of defective graphene sheets is slightly larger than that of the completely rigid flat sheet (D=2), indicating that the presence of SW defects improves the packability of the sheets to a certain extent.²² Also, γ (0.95 $\lesssim \gamma \lesssim$ 0.99) obtained here is lower than that for rigid surfaces ($\gamma=1$), but much higher than that of the self-avoiding tethered membranes ($\gamma=0.8$),^{64,65,66} implying that the graphene sheets maintain a nearly planar yet undulating conformation under the influence of SW defects. Our analyses of the conformational scaling laws highlight the effect of SW defects on the morphology of graphene sheets, contributing to the understanding and design of corrugated defective graphene nanosheets.

Defect-dependent crumpling behavior. To better understand the crumpling behavior of SW defected graphene sheets, we evaluate the evolution of the total potential energy increment ΔPE_{total} , relative shape anisotropy κ^2 , prolateness S, and configuration of the sheets (L=100.6~nm) with different defect ratios p during the crumpling process. It can be found that while ΔPE_{total} of the sheet for any p is relatively steady at the beginning of the crumpling ($0.6 \lesssim \rho_c \leq 1$) and increases significantly at the final stage of the crumpling ($0.133 \leq \rho_c \lesssim 0.2$), the valley of ΔPE_{total} at the middle of the crumpling is observed to be less noticeable with the growth of p (Figure 3a). This can be attributed to the presence of SW defects that weaken the self-adhesion of the graphene sheet (Figure S2), resulting in reduced self-adhering and self-folding behavior of the sheet upon crumpling.³⁰ Moreover, the SW defects considerably increase the angle and dihedral potential energies of the CG graphene model (Figure S3), leading to a significant increase in ΔPE_{total} of the system with a larger p in the final crumpled state (Figure S4), which suggests the more difficult it is to compact the sheet into a spherical shape as p increases.

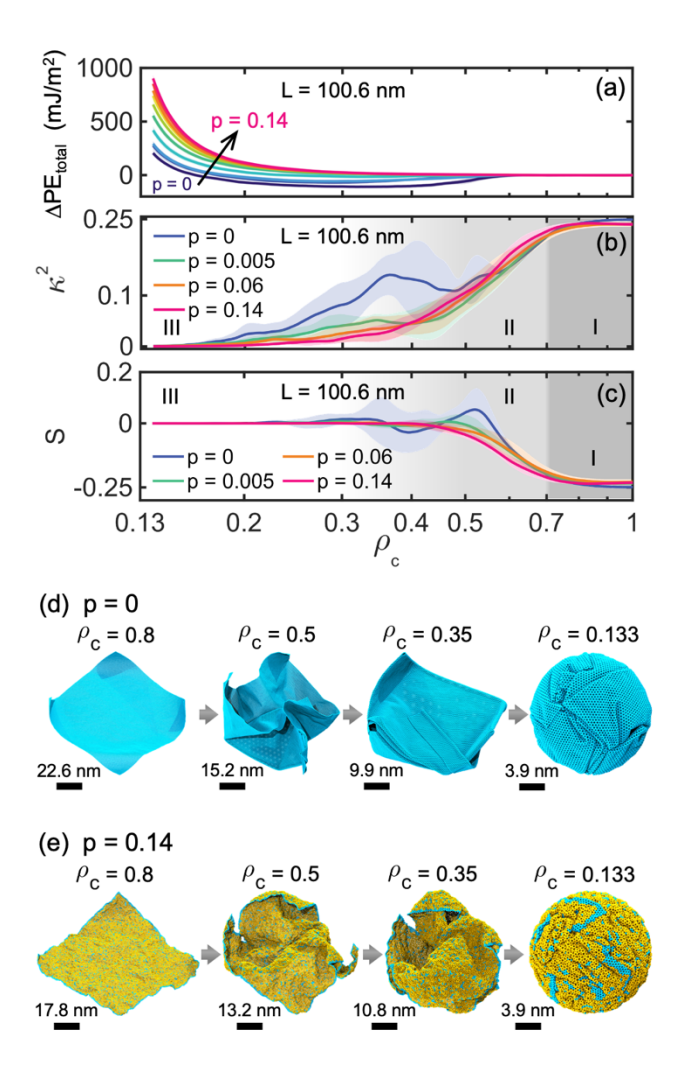


Figure 3. (a) Total potential energy increment per unit area ΔPE_{total} , (b) relative shape anisotropy κ^2 , and (c) prolateness S as a function of the compaction ratio ρ_c for graphene sheets (L=100.6 nm) having various SW defect ratios p ranging from 0 to 0.14. The solid arrow marks the direction of increase of p. Regimes I, II, and III are characterized based on the evolution of κ^2 and S. In particular, $\kappa^2=0.25$ for symmetrical ideal flat sheet and $\kappa^2=0$ for ideal sphere; S=0, $0 < S \le 2$, and $-0.25 \le S < 0$ for spherical, prolate-like, and oblate-like structures, respectively. Shaded areas of the curves correspond to the standard deviation from five independent simulations. Representative configurations of crumpled graphene sheets (L=100.6 nm) for $\rho_c=0.8$, 0.5, 0.35, and 0.133, respectively, with (d) p=0 (pristine) and (e) p=0.14. The gray arrow shows the crumpling process as ρ_c decreases. The black line denotes the scale bar. Details on the calculation of ΔPE_{total} , κ^2 and S are given in the Supporting Information and in previous studies.^{24,30}

The analyses of shape descriptors (i.e., κ^2 describes the symmetry and dimensionality of the model, and S characterizes the degree to which the model deviates from the prolate configuration)^{67,68} reveals that the crumpling process of SW defected graphene sheets can be divided into three regimes, i.e., less bent (0.7 $\lesssim \rho_c \leq$ 1, regime I), intermediate (0.4 \pm 0.1 $\lesssim \rho_c \lesssim$ 0.7, regime II), and highly crumpled (0.133 $\leq \rho_c \lesssim 0.4 \pm 0.1$, regime III) regimes (Figure 3b,c). To be detailed, κ^2 and S are maintained around 0.25 and -0.25, respectively, for all sheets in regime I, where sheets are less bent out of plane at corners but relatively planar in overall configuration (e.g., $\rho_c = 0.8$ in Figure 3d,e). In regime II, all sheets have a continuous decrease in κ^2 and increase in S, representing a significant bending and folding of the sheet during this regime (e.g., $\rho_c = 0.5$ in Figure 3d,e). Notably, κ^2 and S of pristine graphene sheet (p = 0) show considerable rebound and fluctuation in the transition from regime II to III, while those of defective graphene sheets (e.g., p = 0.14) vary smoothly. This is attributed to the fact that the defects weaken the self-adhering and self-folding behaviors of the sheets causing them to form a crumpled configuration without large planar regions (e.g., $\rho_c = 0.35$ in Figure 3d,e).^{24,30} All sheets are highly compacted into spherical shapes in regime III (e.g., $\rho_c = 0.133$ in Figure 3d,e), bringing κ^2 and S to zero. Our analysis of the radial distribution function g(r) of the sheets during the crumpling process further reveals the defect-dependent transition behavior of the system from the initially ordered state to the disordered glassy state (Figure S5). Our simulation results suggest that SW defects control the crumpling process of graphene sheets by diminishing the adhesion behavior of the system, which provides insights into the design of the crumpled system.

Mechanical heterogeneity and internal structure. The local curvature K, von Mises stress σ_v , and cross-section patterns of the crumpled graphene sheet in the final crumpled state ($\rho_c = 0.133$) are evaluated to understand the mechanical heterogeneity and "glass-like" internal structure

of the crumples affected by SW defects. It can be found that both the high curvature and high stress regions of the crumpled system increase significantly with the increase of the SW defect ratios p and coalesce into "dense" networks (Figure 4a,b). Also, the skewed Gaussian-like probability distributions of K and σ_v switch from relatively concentrated at p=0 to relatively wide at p=0.14, and the peaks of the distributions both decrease and shift to larger K and σ_v , respectively, as p increases (Figure 4c,d). These phenomena verify the direct influence of SW defect ratio on the degree of mechanical heterogeneity of the crumpled system, suggesting the presence of pre-stress introduced by the SW defects potentially alters the path of stress propagation during the crumpling process. We emphasize that the mechanical heterogeneity of the crumpled sheet is dominated by the natural distortion of the SW defect lattice (Figure S1), and by the sharp crumples (e.g., bends, developable cones, and stretching ridges) developed along the distorted lattice of the sheet upon crumpling (Figure 4a). Additionally, it is found that the correlation between curvature and stress of the crumpled sheet diminishes as the defect ratio increases (Figure S6).

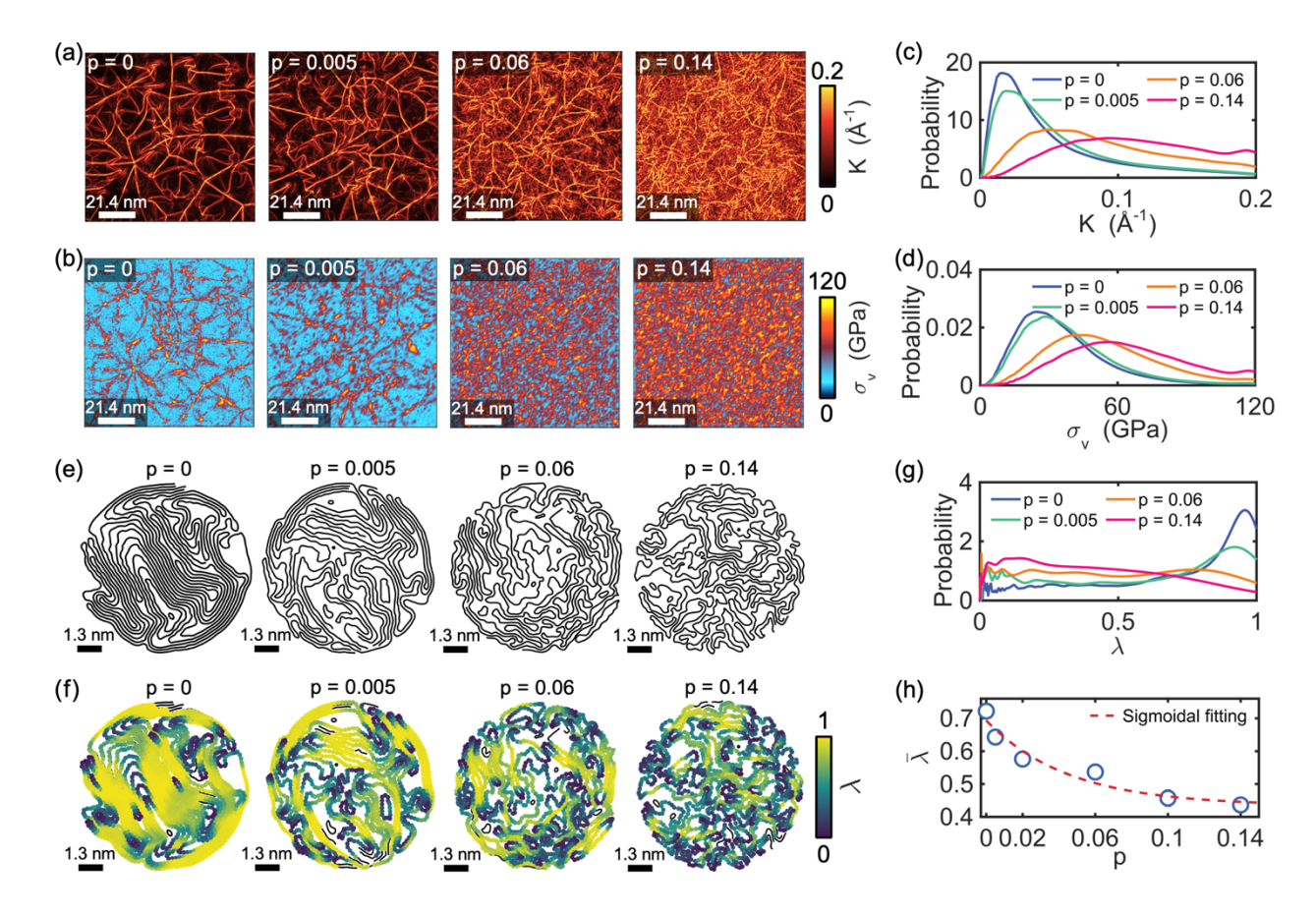


Figure 4. Maps of the local (a) curvature K and (b) von Mises stress σ_v distributions for graphene sheets (L=100.6 nm) with different SW defect ratios p in the final crumpled state (i.e., the crumpled spheres at $\rho_c=0.133$). The local curvatures and von Mises stresses are mapped to a 2D planar model for better visualization. Probability distributions of the (c) K and (d) σ_v for graphene crumpled spheres with different p. (e) Cross-section patterns for graphene crumpled spheres (L=100.6 nm) with varying p. (f) Local order parameter λ and (g) its probability distributions for the cross-section of the graphene crumpled spheres having different defect states. In particular, $0 \le \lambda \le 1$, and a larger (smaller) λ indicates a more (less) crystalline system. (h) Variation of the mean order parameter $\bar{\lambda}$ of the cross-section with p, where the dashed line shows the fitting. The white and black lines denote the scale bar. Details on the calculation of K, σ_v , and λ are given in the Supporting Information and in previous studies. $\frac{25,30,69}{100.00}$

Exploring the cross-section pattern of the crumpled sheet provides valuable insights into its internal structures.^{70,71,72,73,74} Here, the crumpled sphere is cut by a virtual plane passing through its center of mass to obtain the cross-section pattern (Figure S7). It can be observed from Figure

4e that the cross-section of the crumpled spheres gradually changes from the comparatively ordered with lamellar patterns at low SW defect ratios (e.g., p = 0, 0.005) to the disordered patterns at high defect ratios (e.g., p = 0.06, 0.14). This can be interpreted as the sheet with low pforms more lamellar structures upon crumpling due to the significant self-adhering behavior, whereas the system with high p develops more random crumples owing to the distortion of the defect lattice and the weaker self-adhering behavior (Figures 2a and 3). Further, we can quantify the ordered (semicrystalline) and disordered (amorphous) features of the cross-section pattern utilizing local order parameter λ , in case we consider the cross-section pattern of a crumpled sheet as the combination of several polymer chains following a specific configuration. ⁶⁹ It is found that the laminated and overall straight segments in the cross-section pattern have larger λ , in contrast to the segments with distinct folds and undulations that have relatively smaller λ (Figure 4f). Moreover, the segments of large λ decrease with increasing p (Figure 4f) and the increase in p shifts the peak of the probability distribution of λ to smaller λ (Figure 4g). The analysis of the mean order parameter $\bar{\lambda}$ of the entire cross-section pattern shows that $\bar{\lambda}$ decreases with raising p (Figure 4h). This observation suggests that SW defects reduce the "semicrystalline" configuration of the internal structure of the crumpled sheet but lead to more amorphous "glassy" structure, which is influenced by defects upon crumpling process.

In conclusion, we systematically studied the critical role of Stone–Wales (SW) defects on the crumpling behavior and internal structure of graphene sheets employing molecular dynamics (MD) simulations in this study. The conformational characteristics and scaling laws of defective graphene sheets in initial equilibrium, the potential energy and conformational evolutions during the crumpling process, as well as the local curvature, local stresses, and cross-section patterns of defective graphene crumpled spheres are explored at the molecular level, respectively. We find

that the SW defected graphene model based on the previously developed coarse-grained (CG) model⁵⁴ can effectively capture the fundamental conformational features of the sheet under the influence of defects. Due to the defect percolation, the conformational scaling laws for graphene sheets in initial equilibrium are remarkably influenced by SW defects in the regime of low defect ratio $(p \leq 0.03)$, while they become less sensitive (saturated) in the high defect ratio regime $(p \geq$ 0.03). Moreover, SW defects enhance the sheet's in-plane elastic and out-of-plane bending potentials, making it more resistant to being compacted into a crumpled sphere, which nevertheless weakens the self-adhering and self-folding behavior of the graphene sheet during the crumpling process. Remarkably, SW defects increase the degree of mechanical heterogeneity and diminish the correlation between the local curvature and stress of the graphene crumpled spheres. It is interesting to note that the cross-section patterns of crumpled spheres vary from ordered lamellar to disordered folds with increasing SW defect ratios, implying that the defects lead to an amorphous internal structure. We believe such a fundamental understanding of crumpling behavior for defective graphene sheet can serve as a platform and provide more insights into the crumpled materials design with predictable internal structures.

ASSOCIATED CONTENT

Supporting Information.

Further details of CG model, MD simulations, property calculations, as well as additional analyses on the crumpled SW defected graphene sheets.

AUTHOR INFORMATION

Corresponding Author

Wenjie Xia – Department of Civil, Construction and Environmental Engineering, North Dakota State University, Fargo, North Dakota 58108, United States; Materials and Nanotechnology, North Dakota State University, Fargo, North Dakota 58108, United States; orcid.org/0000-0001-

7870-0128; Email: wenjie.xia@ndsu.edu

Authors

Yangchao Liao – Department of Civil, Construction and Environmental Engineering, North Dakota State University, Fargo, North Dakota 58108, United States; orcid.org/0000-0001-7154-3916

Zhaofan Li – Department of Civil, Construction and Environmental Engineering, North Dakota State University, Fargo, North Dakota 58108, United States; orcid.org/0000-0001-7868-413X Andrew B. Croll – Department of Physics, North Dakota State University, Fargo, North Dakota 58108, United States; Materials and Nanotechnology, North Dakota State University, Fargo, North Dakota 58108, United States; orcid.org/0000-0002-6890-3084

Author Contributions

Y.L. and W.X. conceived and designed the research. Y.L. performed the MD simulations and wrote the original draft. Y.L., Z.L., A.B.C., and W.X. contributed to the data analyses. A.B.C. and W.X. supervised the project. All authors have contributed to and approved the final version of the manuscript.

Notes

The authors declare no competing financial interest.

ACKNOWLEDGMENT

The authors acknowledge the support from the Army Research Office (Award No. W911NF2010208). The authors also acknowledge support from the Department of Civil, Construction and Environmental Engineering and College of Engineering at North Dakota State University (NDSU). This work used resources of the Center for Computationally Assisted Science and Technology (CCAST) at North Dakota State University, which were made possible in part by NSF MRI Award No. 2019077.

REFERENCES

- (1) Saito, R.; Fujita, M.; Dresselhaus, G.; Dresselhaus, M. S. Electronic Structure of Chiral Graphene Tubules. *Appl. Phys. Lett.* **1992**, *60* (18), 2204–2206. https://doi.org/10.1063/1.107080.
- (2) Sakhaee-Pour, A. Elastic Buckling of Single-Layered Graphene Sheet. *Comput. Mater. Sci.* **2009**, *45* (2), 266–270. https://doi.org/https://doi.org/10.1016/j.commatsci.2008.09.024.
- (3) Balandin, A. A. Thermal Properties of Graphene and Nanostructured Carbon Materials.

 Nature Materials. 2011, pp 569–581. https://doi.org/10.1038/nmat3064.
- (4) Novoselov, K. S.; Geim, A. K.; Morozov, S. V.; Jiang, D.; Zhang, Y.; Dubonos, S. V.; Grigorieva, I. V.; Firsov, A. A. Electric Field in Atomically Thin Carbon Films. *Science* (80-.). 2004, 306 (5696), 666–669. https://doi.org/10.1126/science.1102896.
- (5) Rao, C. N. R.; Matte, H. S. S. R.; Subrahmanyam, K. S.; Maitra, U. Unusual Magnetic Properties of Graphene and Related Materials. *Chemical Science*. 2012, pp 45–52. https://doi.org/10.1039/c1sc00726b.
- (6) Deng, S.; Berry, V. Wrinkled, Rippled and Crumpled Graphene: An Overview of Formation Mechanism, Electronic Properties, and Applications. *Materials Today*. Elsevier B.V. May 1, 2016, pp 197–212. https://doi.org/10.1016/j.mattod.2015.10.002.
- (7) Zang, J.; Ryu, S.; Pugno, N.; Wang, Q.; Tu, Q.; Buehler, M. J.; Zhao, X. Multifunctionality and Control of the Crumpling and Unfolding of Large-Area Graphene. *Nat. Mater.* **2013**, *12* (4), 321–325. https://doi.org/10.1038/nmat3542.

- (8) Xu, Z.; Buehler, M. J. Geometry Controls Conformation of Graphene Sheets: Membranes, Ribbons, and Scrolls. ACS Nano 2010, 4 (7), 3869–3876. https://doi.org/10.1021/nn100575k.
- (9) Banhart, F.; Kotakoski, J.; Krasheninnikov, A. V. Structural Defects in Graphene. *ACS Nano*. November 23, 2011, pp 26–41. https://doi.org/10.1021/nn102598m.
- (10) Zhang, W.; Kim, M.; Cheng, R.; Lu, W. C.; Zhang, H. X.; Ho, K. M.; Wang, C. Z. Defect Interaction and Deformation in Graphene. J. Phys. Chem. C 2020, 124 (4), 2370–2378. https://doi.org/10.1021/acs.jpcc.9b10622.
- (11) Thiemann, F. L.; Rowe, P.; Zen, A.; Müller, E. A.; Michaelides, A. Defect-Dependent Corrugation in Graphene. *Nano Lett.* **2021**, *21* (19), 8143–8150. https://doi.org/10.1021/acs.nanolett.1c02585.
- (12) Cranford, S.; Sen, D.; Buehler, M. J. Meso-Origami: Folding Multilayer Graphene Sheets. *Appl. Phys. Lett.* **2009**, *95* (12), 123121. https://doi.org/10.1063/1.3223783.
- (13) Lechenault, F.; Thiria, B.; Adda-Bedia, M. Mechanical Response of a Creased Sheet. *Phys. Rev. Lett.* **2014**, *112* (24). https://doi.org/10.1103/PhysRevLett.112.244301.
- (14) Cerda, E.; Chaleb, S.; Melo, F.; Mahadevan, L. Conical Dislocations in Crumpling. *Nature* **1999**, *401* (6748), 46–49. https://doi.org/10.1038/43395.
- (15) Lobkovsky, A.; Gentges, S.; Li, H.; Morse, D.; Witten, T. A. Scaling Properties of Stretching Ridges in a Crumpled Elastic Sheet. *Science (80-.)*. **1995**, *270* (5241), 1482–1485. https://doi.org/10.1126/science.270.5241.1482.

- (16) El Rouby, W. M. A. Crumpled Graphene: Preparation and Applications. *RSC Adv.* 2015, 5(82), 66767–66796. https://doi.org/10.1039/c5ra10289h.
- (17) Chang, C.; Song, Z.; Lin, J.; Xu, Z. How Graphene Crumples Are Stabilized? *RSC Adv*.
 2013, 3 (8), 2720–2726. https://doi.org/10.1039/c2ra21563b.
- (18) Liu, Q.; Huang, J.; Xu, B. Evaporation-Driven Crumpling and Assembling of Two-Dimensional (2D) Materials: A Rotational Spring Mechanical Slider Model. *J. Mech. Phys. Solids* **2019**, *133*. https://doi.org/10.1016/j.jmps.2019.103722.
- (19) Liao, Y.; Li, Z.; Fatima; Xia, W. Size-Dependent Structural Behaviors of Crumpled Graphene Sheets. *Carbon N. Y.* **2021**, *174*, 148–157. https://doi.org/10.1016/j.carbon.2020.12.006.
- (20) Becton, M.; Zhang, L.; Wang, X. Mechanics of Graphyne Crumpling. *Phys. Chem. Chem. Phys.* **2014**, *16* (34), 18233–18240. https://doi.org/10.1039/c4cp02400a.
- (21) Giordanelli, I.; Mendoza, M.; Andrade, J. S.; Gomes, M. A. F.; Herrmann, H. J. Crumpling Damaged Graphene. *Sci. Rep.* **2016**, *6*. https://doi.org/10.1038/srep25891.
- (22) Cranford, S. W.; Buehler, M. J. Packing Efficiency and Accessible Surface Area of Crumpled Graphene. *Phys. Rev. B Condens. Matter Mater. Phys.* **2011**, *84* (20), 205451. https://doi.org/10.1103/PhysRevB.84.205451.
- (23) Becton, M.; Zhang, L.; Wang, X. On the Crumpling of Polycrystalline Graphene by Molecular Dynamics Simulation. *Phys. Chem. Chem. Phys.* **2015**, *17* (9), 6297–6304. https://doi.org/10.1039/c4cp05813e.

- (24) Liao, Y.; Li, Z.; Ghazanfari, S.; Fatima; Croll, A. B.; Xia, W. Understanding the Role of Self-Adhesion in Crumpling Behaviors of Sheet Macromolecules. *Langmuir* **2021**, *37* (28), 8627–8637. https://doi.org/10.1021/acs.langmuir.1c01545.
- (25) Croll, A. B.; Liao, Y.; Li, Z.; Jayawardana, W. M. A.; Elder, T.; Xia, W. Sticky Crumpled Matter. *Matter* **2022**, *5* (6), 1792–1805. https://doi.org/10.1016/j.matt.2022.04.029.
- Baimova, J. A.; Liu, B.; Dmitriev, S. V.; Srikanth, N.; Zhou, K. Mechanical Properties of Bulk Carbon Nanostructures: Effect of Loading and Temperature. *Phys. Chem. Chem. Phys.*2014, 16 (36), 19505–19513. https://doi.org/10.1039/c4cp01952k.
- (27) Koltonow, A. R.; Luo, C.; Luo, J.; Huang, J. Graphene Oxide Sheets in Solvents: To Crumple or Not to Crumple? *ACS Omega* **2017**, *2* (11), 8005–8009. https://doi.org/10.1021/acsomega.7b01647.
- (28) Li, P.; Wang, S.; Meng, F.; Wang, Y.; Guo, F.; Rajendran, S.; Gao, C.; Xu, Z.; Xu, Z. Conformational Scaling Relations of Two-Dimensional Macromolecular Graphene Oxide in Solution. *Macromolecules* 2020, 53 (23), 10421–10430. https://doi.org/10.1021/acs.macromol.0c01425.
- (29) Ma, X.; Zachariah, M. R.; Zangmeister, C. D. Crumpled Nanopaper from Graphene Oxide.

 Nano Lett. 2012, 12 (1), 486–489. https://doi.org/10.1021/nl203964z.
- (30) Liao, Y.; Li, Z.; Nie, W.; Xia, W. Effect of Reconstructed Vacancy Defects on the Crumpling Behavior of Graphene Sheets. *Forces Mech.* **2022**, *6*, 100057. https://doi.org/10.1016/j.finmec.2021.100057.

- (31) Cui, L.; Du, X.; Wei, G.; Feng, Y. Thermal Conductivity of Graphene Wrinkles: A Molecular Dynamics Simulation. *J. Phys. Chem. C* **2016**, *120* (41), 23807–23812. https://doi.org/10.1021/acs.jpcc.6b07162.
- (32) Luo, J.; Jang, H. D.; Sun, T.; Xiao, L.; He, Z.; Katsoulidis, A. P.; Kanatzidis, M. G.; Gibson, J. M.; Huang, J. Compression and Aggregation-Resistant Particles of Crumpled Soft Sheets. *ACS Nano* **2011**, *5* (11), 8943–8949. https://doi.org/10.1021/nn203115u.
- (33) Zhu, W.; Low, T.; Perebeinos, V.; Bol, A. A.; Zhu, Y.; Yan, H.; Tersoff, J.; Avouris, P. Structure and Electronic Transport in Graphene Wrinkles. *Nano Lett.* **2012**, *12* (7), 3431–3436. https://doi.org/10.1021/nl300563h.
- (34) Wang, Y.; Meng, Z. Mechanical and Viscoelastic Properties of Wrinkled Graphene Reinforced Polymer Nanocomposites Effect of Interlayer Sliding within Graphene Sheets. *Carbon N. Y.* **2021**, *177*, 128–137. https://doi.org/10.1016/j.carbon.2021.02.071.
- Ramanathan, T.; Abdala, A. A.; Stankovich, S.; Dikin, D. A.; Herrera-Alonso, M.; Piner, R. D.; Adamson, D. H.; Schniepp, H. C.; Chen, X.; Ruoff, R. S.; Nguyen, S. T.; Aksay, I. A.; Prud'Homme, R. K.; Brinson, L. C. Functionalized Graphene Sheets for Polymer Nanocomposites. *Nat. Nanotechnol.* 2008, 3 (6), 327–331. https://doi.org/10.1038/nnano.2008.96.
- (36) Wang, Y.; Yang, R.; Shi, Z.; Zhang, L.; Shi, D.; Wang, E.; Zhang, G. Super-Elastic Graphene Ripples for Flexible Strain Sensors. *ACS Nano* **2011**, *5* (5), 3645–3650. https://doi.org/10.1021/nn103523t.
- (37) Miller, J. R.; Outlaw, R. A.; Holloway, B. C. Graphene Double-Layer Capacitor with Ac

- Line-Filtering Performance. *Science* (80-.). **2010**, 329 (5999), 1637–1639. https://doi.org/10.1126/science.1194372.
- (38) Zhu, Y.; Murali, S.; Stoller, M. D.; Ganesh, K. J.; Cai, W.; Ferreira, P. J.; Pirkle, A.; Wallace, R. M.; Cychosz, K. A.; Thommes, M.; Su, D.; Stach, E. A.; Ruoff, R. S. Carbon-Based Supercapacitors Produced by Activation of Graphene. *Science* (80-.). 2011, 332 (6037), 1537–1541. https://doi.org/10.1126/science.1200770.
- (39) Luo, J.; Jang, H. D.; Huang, J. Effect of Sheet Morphology on the Scalability of Graphene-Based Ultracapacitors. *ACS Nano* **2013**, 7 (2), 1464–1471. https://doi.org/10.1021/nn3052378.
- (40) Chen, Y.; Guo, F.; Jachak, A.; Kim, S. P.; Datta, D.; Liu, J.; Kulaots, I.; Vaslet, C.; Jang, H. D.; Huang, J.; Kane, A.; Shenoy, V. B.; Hurt, R. H. Aerosol Synthesis of Cargo-Filled Graphene Nanosacks. *Nano Lett.* 2012, 12 (4), 1996–2002. https://doi.org/10.1021/nl2045952.
- (41) Dou, X.; Koltonow, A. R.; He, X.; Jang, H. D.; Wang, Q.; Chung, Y. W.; Huang, J. Self-Dispersed Crumpled Graphene Balls in Oil for Friction and Wear Reduction. *Proc. Natl. Acad. Sci. U. S. A.* **2016**, *113* (6), 1528–1533. https://doi.org/10.1073/pnas.1520994113.
- (42) Stone, A. J.; Wales, D. J. Theoretical Studies of Icosahedral C60 and Some Related Species. *Chem. Phys. Lett.* **1986**, *128* (5–6), 501–503. https://doi.org/10.1016/0009-2614(86)80661-3.
- (43) Ma, J.; Alfè, D.; Michaelides, A.; Wang, E. Stone-Wales Defects in Graphene and Other Planar s P2 -Bonded Materials. *Phys. Rev. B Condens. Matter Mater. Phys.* **2009**, *80* (3).

- https://doi.org/10.1103/PhysRevB.80.033407.
- (44) Amorim, R. G.; Fazzio, A.; Antonelli, A.; Novaes, F. D.; Da Silva, A. J. R. Divacancies in Graphene and Carbon Nanotubes. *Nano Lett.* **2007**, *7* (8), 2459–2462. https://doi.org/10.1021/nl071217v.
- (45) Song, Z.; Artyukhov, V. I.; Wu, J.; Yakobson, B. I.; Xu, Z. Defect-Detriment to Graphene Strength Is Concealed by Local Probe: The Topological and Geometrical Effects. *ACS Nano* **2015**, *9* (1), 401–408. https://doi.org/10.1021/nn505510r.
- (46) Yazyev, O. V.; Louie, S. G. Topological Defects in Graphene: Dislocations and Grain Boundaries. *Phys. Rev. B Condens. Matter Mater. Phys.* **2010**, *81* (19). https://doi.org/10.1103/PhysRevB.81.195420.
- (47) Tian, W.; Li, W.; Yu, W.; Liu, X. A Review on Lattice Defects in Graphene: Types Generation Effects and Regulation. *Micromachines*. 2017. https://doi.org/10.3390/mi8050163.
- (48) Datt Bhatt, M.; Kim, H.; Kim, G. Various Defects in Graphene: A Review. *RSC Adv.* **2022**, *12*, 21520–21547. https://doi.org/10.1039/d2ra01436j.
- (49) Shi, T.; Peng, Q.; Bai, Z.; Gao, F.; Jovanovic, I. Proton Irradiation of Graphene: Insights from Atomistic Modeling. *Nanoscale* **2019**, *11* (43), 20754–20765. https://doi.org/10.1039/c9nr06502d.
- (50) Krasheninnikov, A. V.; Banhart, F. Engineering of Nanostructured Carbon Materials with Electron or Ion Beams. *Nature Materials*. 2007, pp 723–733.

- https://doi.org/10.1038/nmat1996.
- Yoon, K.; Rahnamoun, A.; Swett, J. L.; Iberi, V.; Cullen, D. A.; Vlassiouk, I. V.; Belianinov, A.; Jesse, S.; Sang, X.; Ovchinnikova, O. S.; Rondinone, A. J.; Unocic, R. R.; Van Duin, A. C. T. Atomistic-Scale Simulations of Defect Formation in Graphene under Noble Gas Ion Irradiation. *ACS Nano* 2016, 10 (9), 8376–8384. https://doi.org/10.1021/acsnano.6b03036.
- (52) Toh, C. T.; Zhang, H.; Lin, J.; Mayorov, A. S.; Wang, Y. P.; Orofeo, C. M.; Ferry, D. B.; Andersen, H.; Kakenov, N.; Guo, Z.; Abidi, I. H.; Sims, H.; Suenaga, K.; Pantelides, S. T.; Özyilmaz, B. Synthesis and Properties of Free-Standing Monolayer Amorphous Carbon. *Nature* 2020, 577 (7789), 199–203. https://doi.org/10.1038/s41586-019-1871-2.
- (53) Chen, C.; Duan, F. L. Effect of Functional Groups on Crumpling Behavior and Structure of Graphene Oxide. *Wuli Xuebao/Acta Phys. Sin.* **2020**, *69* (19). https://doi.org/10.7498/aps.69.20200651.
- (54) Ruiz, L.; Xia, W.; Meng, Z.; Keten, S. A Coarse-Grained Model for the Mechanical Behavior of Multi-Layer Graphene. *Carbon N. Y.* **2015**, *82* (C), 103–115. https://doi.org/10.1016/j.carbon.2014.10.040.
- (55) Chen, D.; Zheng, Y.; Liu, L.; Zhang, G.; Chen, M.; Jiao, Y.; Zhuang, H. Stone–Wales Defects Preserve Hyperuniformity in Amorphous Two-Dimensional Networks. *Proc. Natl. Acad. Sci. U. S. A.* **2021**, *118* (3). https://doi.org/10.1073/pnas.2016862118.
- (56) Wang, W. N.; Jiang, Y.; Biswas, P. Evaporation-Induced Crumpling of Graphene Oxide Nanosheets in Aerosolized Droplets: Confinement Force Relationship. *J. Phys. Chem. Lett.*

- **2012**, 3 (21), 3228–3233. https://doi.org/10.1021/jz3015869.
- (57) Yang, Y.; Teng, B. The Affection on the Nature of Percolation by Concentration of Pentagon-Heptagon Defects in Graphene Lattice. *Chinese Phys. B* **2018**, *27* (10). https://doi.org/10.1088/1674-1056/27/10/106401.
- (58) Tarasevich, Y. Y.; Laptev, V. V.; Vygornitskii, N. V.; Lebovka, N. I. Impact of Defects on Percolation in Random Sequential Adsorption of Linear K-Mers on Square Lattices. *Phys. Rev. E - Stat. Nonlinear, Soft Matter Phys.* 2015, 91 (1). https://doi.org/10.1103/PhysRevE.91.012109.
- (59) Zhukov, D. O.; Andrianova, E. G.; Lesko, S. A. The Influence of a Network's Spatial Symmetry, Topological Dimension, and Density on Its Percolation Threshold. *Symmetry* (*Basel*). **2019**, *11* (7). https://doi.org/10.3390/sym11070920.
- (60) Juba, D.; Audus, D. J.; Mascagni, M.; Douglas, J. F.; Keyrouz, W. ZENO: Software for Calculating Hydrodynamic, Electrical, and Shape Properties of Polymer and Particle Suspensions. J. Res. Natl. Inst. Stand. Technol. 2017, 122. https://doi.org/10.6028/JRES.122.020.
- (61) Pang, Z.; Deng, B.; Liu, Z.; Peng, H.; Wei, Y. Defects Guided Wrinkling in Graphene on Copper Substrate. *Carbon N. Y.* **2019**, *143*, 736–742. https://doi.org/10.1016/j.carbon.2018.11.059.
- (62) Lusk, M. T.; Carr, L. D. Nanoengineering Defect Structures on Graphene. *Phys. Rev. Lett.* 2008, 100 (17), 175503. https://doi.org/10.1103/PhysRevLett.100.175503.

- (63) Knauert, S. T.; Douglas, J. F.; Starr, F. W. Morphology and Transport Properties of Two-Dimensional Sheet Polymers. *Macromolecules* 2010, 43 (7), 3438–3445. https://doi.org/10.1021/ma902081m.
- (64) Nelson, D.; Piran, T.; Weinberg, S. *Statistical Mechanics of Membranes and Surfaces*; 2004. https://doi.org/10.1142/5473.
- (65) Kantor, Y.; Kardar, M.; Nelson, D. R. Statistical Mechanics of Tethered Surfaces. *Phys. Rev. Lett.* **1986**, *57* (7), 791–794. https://doi.org/10.1103/PhysRevLett.57.791.
- (66) Kantor, Y.; Kardar, M.; Nelson, D. R. Tethered Surfaces: Statics and Dynamics. *Phys. Rev.*A 1987, 35 (7), 3056–3071. https://doi.org/10.1103/PhysRevA.35.3056.
- (67) Arkin, H.; Janke, W. Gyration Tensor Based Analysis of the Shapes of Polymer Chains in an Attractive Spherical Cage. *J. Chem. Phys.* **2013**, *138* (5). https://doi.org/10.1063/1.4788616.
- (68) E. Theodorakis, P.; G. Fytas, N. Molecular Dynamics Simulations of Bottle-Brush Polymers with a Flexible Backbone under Theta and Good Solvent Conditions. *Am. J. Condens. Matter Phys.* **2012**, *2* (4), 101–108. https://doi.org/10.5923/j.ajcmp.20120204.05.
- (69) Verho, T.; Paajanen, A.; Vaari, J.; Laukkanen, A. Crystal Growth in Polyethylene by Molecular Dynamics: The Crystal Edge and Lamellar Thickness. *Macromolecules* 2018, 51 (13), 4865–4873. https://doi.org/10.1021/acs.macromol.8b00857.
- (70) Tallinen, T.; Ström, J. A.; Timonen, J. The Effect of Plasticity in Crumpling of Thin Sheets.

 Nat. Mater. 2009, 8 (1), 25–29. https://doi.org/10.1038/nmat2343.

- (71) Cambou, A. D.; Menon, N. Three-Dimensional Structure of a Sheet Crumpled into a Ball.
 Proc. Natl. Acad. Sci. U. S. A. 2011, 108 (36), 14741–14745.
 https://doi.org/10.1073/pnas.1019192108.
- (72) Lin, Y. C.; Sun, J. M.; Yang, H. W.; Hwu, Y.; Wang, C. L.; Hong, T. M. X-Ray Tomography of a Crumpled Plastoelastic Thin Sheet. *Phys. Rev. E Stat. Nonlinear, Soft Matter Phys.* **2009**, *80* (6). https://doi.org/10.1103/PhysRevE.80.066114.
- (73) Martoïa, F.; Orgéas, L.; Dumont, P. J. J.; Bloch, J. F.; Flin, F.; Viguié, J. Crumpled Paper Sheets: Low-Cost Biobased Cellular Materials for Structural Applications. *Mater. Des.* 2017, 136, 150–164. https://doi.org/10.1016/j.matdes.2017.09.031.
- (74) Vliegenthart, G. A.; Gompper, G. Forced Crumpling of Self-Avoiding Elastic Sheets. *Nat. Mater.* **2006**, *5* (3), 216–221. https://doi.org/10.1038/nmat1581.

For Table of Content use only

